

# Detecting Irregular Network Activity with Adversarial Learning and Expert Feedback

Gopikrishna Rathinavel  
Virginia Tech  
Blacksburg, VA  
rgopikrishna@vt.edu

Nikhil Muralidhar  
Stevens Institute of Technology  
Hoboken, NJ  
nmurali1@stevens.edu

Timothy O'Shea  
DeepSig Inc & Virginia Tech  
Arlington, VA  
tim@deepsig.io

Naren Ramakrishnan  
Virginia Tech  
Arlington, VA  
naren@cs.vt.edu

**Abstract**—Anomaly detection is a ubiquitous and challenging task, relevant across many disciplines. With the vital role communication networks play in our daily lives, the security of these networks is imperative for the smooth functioning of society. To this end, we propose a novel self-supervised deep learning framework CAAD for anomaly detection in wireless communication systems. Specifically, CAAD employs contrastive learning in an adversarial setup to learn effective representations of normal and anomalous behavior in wireless networks. We conduct rigorous performance comparisons of CAAD with several state-of-the-art anomaly detection techniques and verify that CAAD yields a mean performance improvement of 92.84%. Additionally, we also augment CAAD enabling it to systematically incorporate expert feedback through a novel contrastive learning feedback loop to improve the learned representations and thereby reduce prediction uncertainty (CAAD-EF). We view CAAD-EF as a novel, holistic, and widely applicable solution to anomaly detection. Our source code and data are available online<sup>1</sup>

**Index Terms**—anomaly detection, generative neural networks, wireless, self-supervised learning, contrastive learning, expert feedback

## I. INTRODUCTION

Wireless communications systems form an essential component of cyber-physical systems in urban environments along with the electric grid and the transportation network. These wireless communication systems and networks enable us to access the internet, and connect with others remotely, thereby serving as a vital means for human interaction. Further, they connect hundreds or thousands of sensors, applications, industrial networks, critical communications systems, and other infrastructure. Hence, state monitoring and detection of irregular activity in wireless networks are essential to ensuring robust and resilient system operational capabilities.

The *electromagnetic spectrum* (simply referred to as ‘the spectrum’) is the information highway through which most modern forms of electronic communication occur. Parts of the spectrum are grouped into ‘bands’ (based on the wavelength) which can be thought of as analogous to lanes on the highway. Specific regions (i.e., lanes) of the spectrum are reserved for specific types of communication (e.g., radio communication, broadcast television) based on frequency. The entire spectrum ranges from 3Hz-300EHz and the typical range used for *wireless communication* today is 30KHz-28GHz.

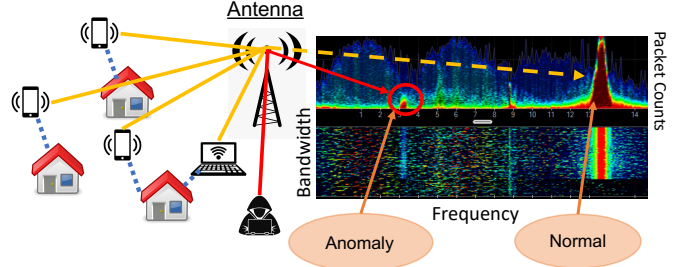


Fig. 1. Irregular Activity in Wireless Communication Systems. [1]

*Spectrum access activity* in wireless systems carries rich information which can indicate underlying activity of physical device presence, activity and behaviors corresponding to security threats and intrusions, jamming attempts, device malfunctioning, interference, illicit transmissions, and a host of other activities (see Fig. 1). Data corresponding to spectrum access activity information has been explored in wireless intrusion detection systems (WIDS) in a very limited context and most of the systems in use today for detecting anomalous network activity, are highly application specific and focus on specialized feature engineering, detector engineering, and signal-specific digital signal processing (DSP) engineering. Such systems are not generalizable, are highly sensitive to minor variations in system characteristics and are costly to maintain due to the requirements of rich feature engineering.

Hence in this work, we have developed a generic and powerful unsupervised anomaly detection framework and demonstrated its prowess in the context of wireless network anomalies. Specifically, we propose a novel solution to anomaly detection (AD), *Contrastive Adversarial Anomaly Detection* (CAAD) which applies contrastive learning (CL) in an adversarial setup. We also augment CAAD with the ability to incorporate expert feedback (EF) to improve the quality of its learned representations for AD. We call this model CAAD-EF (CAAD with expert feedback). To the best of our knowledge, we are the first to propose such a powerful yet flexible AD framework that applies contrastive learning paradigms in an adversarial setup with the ability to incorporate expert feedback via contrastive learning to improve its learned representations and reduce prediction uncertainty.

Our contributions are as follows:

<sup>1</sup><https://github.com/rgopikrishna-vt/CAAD>

- We propose CAAD, a novel method for AD which utilizes contrastive learning and generative adversarial networks (GAN). We demonstrate that our proposed model is able to significantly outperform state-of-the-art (SOTA) models on AD in wireless networks and standard datasets. To the best of our knowledge, CAAD is the first model to use a combination of CL and adversarial learning for AD.
- We propose CAAD-EF, which is another novel model supplemental to CAAD, which further enables us to incorporate expert feedback via contrastive learning and uncertainty quantification using Monte Carlo dropouts. To the best of our knowledge, our framework is the first successful undertaking to utilize contrastive learning to incorporate expert feedback.
- Finally, we highlight the importance of various facets of CAAD-EF through rigorous qualitative, quantitative, and ablation analyses.

## II. RELATED WORK

Many ML approaches have been developed for anomaly detection across diverse applications. The recent resurgence of deep learning techniques demonstrating their effectiveness across a wide variety of domains has led to the development of many novel and powerful modeling paradigms like generative adversarial networks (GAN) [2], self-supervised representation learning [3] and contrastive learning (CL) [4]. *Contrastive Learning (CL)* imposes structure on the latent space by encouraging similarity in representations learned for *related* instances and dissimilarity in representations for unrelated instances. Such techniques have proven effective, especially when combined with self-supervised learning [5], [6] and also with labeled data [7]. CL has demonstrated promising results in image recognition tasks. However, most of these efforts focus on improving representation learning performance on traditional classification tasks and do not specifically focus on AD. *Generative Adversarial Networks (GANs)* [2] are a powerful generative learning paradigm grounded in an adversarial training setup. However, they are fraught with training instability. Recently, improvements have been proposed to stabilize the GAN training setup by employing *Wasserstien* distance functions [8] and gradient penalties on the learned weights.

**Deep Learning for Anomaly Detection:** The aforementioned developments in deep learning have led to techniques such as autoencoders and GANs being employed for the ubiquitous and challenging problem of AD. Specifically, in [9], a deep robust autoencoder (*Robust AE*) model is proposed, inspired by the Robust Principal Component Analysis technique, for AD with noisy training data. However, this methodology by design requires knowledge of a subset of anomalies during model training and may be considered semi-supervised, and is not directly related to our context of unsupervised AD. Recently, another line of AD research [10] proposes employing DCGAN [2] for unsupervised AD. The authors then build upon their previous work to propose *fAnoGAN* [11], a two-step encoder-decoder architecture based on DCGANs where the encoder (trained separately) learns to invert the mapping

learned by the Generator (i.e., decoder) of the DCGAN model. We employ *fAnoGAN* as one of the baselines for empirical comparison.

**Contrastive Learning for Anomaly Detection:** There are multiple reports of contrastive learning being utilized for AD. *Masked Contrastive Learning* [12] is a supervised method that varies the weights of different classes in the contrastive loss function to produce good representations that separate each class. Even though this method shows promise, it requires knowledge of anomaly labels. *Contrasting Shifted Instances (CSI)* [13] and *Mean Shifted Contrastive Loss* [14] are two unsupervised AD methods based on CL. CSI investigates the power of self-supervised CL for detecting out-of-distribution (OOD) data by using distributionally shifted variations of input data. We employ CSI as one of our baselines. *Mean Shifted Contrastive Loss* applies a contrastive loss modified using the mean representation on representations generated using models pre-trained on ImageNet data. However, this model is not useful for wireless AD as it is pre-trained on a particular kind of data. Also, none of these methods provide a means to incorporate expert feedback.

**Incorporating Expert Feedback:** The solutions presented in [15]–[19] all employ human feedback in various ways. Active Anomaly Discovery (AAD) [15] is designed to operate in an anomaly exploration loop where the algorithm selects data to be presented to experts and also provides a means to incorporate feedback into the model. However, its performance is dependent on the number of feedback loops that can be afforded. Hence, such a method could not be applied to wireless AD where the volume of input data is really high. RAMODO [17], combines representation learning and outlier detection in a single objective function. It utilizes pseudo labels generated by other state-of-the-art outlier detection methods and Chebyshev’s inequality. This dependence on other methods to generate pseudo labels can sometimes be unreliable in cases where state-of-the-art outlier detection methods perform poorly. SAAD [16], DevNet [18] and DPLAN [19] are semi-supervised methods, all of which require minimal labeled anomalies and are not suitable for our problem.

The advantage of using contrastive learning for AD is that it can be utilized in a self-supervised setup. That is, we can augment the training samples to generate anomalous samples that are very close to the training distribution and utilize them as negative samples in contrastive loss. This allows our model to detect unseen anomalies effectively. Also, the penultimate layer of the GAN discriminators has recently been shown to act as good representations of the input data [11], [20]–[22]. Hence, the combination of these powerful techniques, CL and GAN serve well for our AD task. None of the related approaches outlined above have developed AD techniques that combine the aforementioned techniques for AD. Also, none of the state-of-the-art related AD approaches provide a means to incorporate expert feedback via contrastive learning.

### III. BACKGROUND

We propose CAAD and CAAD-EF which employ techniques such as adversarial learning, contrastive learning (CL) and uncertainty quantification (UQ). We shall now briefly introduce these concepts before detailing the full CAAD-EF framework in section IV.

#### A. Generative Adversarial Networks (GAN)

GANs are a class of generative models where the learning problem is formulated as a game between two neural networks, namely the *generator* (G) and the *discriminator* (D). The problem setup of GANs comprises the generator learning to transform inputs sampled from a noise distribution into a distribution  $P_f$  such that it resembles the true data distribution  $P_r$ . Essentially, the generator is trained to *fool* the discriminator while the discriminator is tasked with distinguishing between *fake* samples  $\tilde{x} \sim P_f$  generated by G and *real* samples  $x \sim P_r$ . The traditional GAN [2] setup minimizes the Jensen-Shannon (JS) divergence between  $P_r$  and  $P_f$ . However, this divergence is not continuous with respect to the parameters of G, leading to training instabilities. Wasserstein GAN [8] (WGAN) was proposed to address this issue. WGAN employs Earth-Mover distance (instead of the JS divergence) which under mild assumptions does not have discontinuities and is almost universally differentiable. Consider the discriminator (also termed the *critic*<sup>2</sup> in WGAN) D parameterized by  $\Omega$  and generator G parameterized by  $\theta$ . Eq. 1 depicts the WGAN loss function where  $D$  is parameterized by  $\Omega \in \mathcal{B}$ , where  $\mathcal{B}$  is the set of 1-Lipschitz functions.

$$L^w = \min_{\theta} \max_{\Omega \in \mathcal{B}} \mathbb{E}_{x \sim P_r} [D_{\Omega}(x)] - \mathbb{E}_{\tilde{x} \sim P_f} [D_{\Omega}(\tilde{x})] \quad (1)$$

Enforcing the 1-Lipschitz constraint on  $D_{\Omega}$  has been found to be challenging. On the basis of the property that a function is 1-Lipschitz if and only if it has a norm no greater than 1 everywhere, [23] proposed a solution of augmenting the WGAN loss with a soft constraint enforcing that the norm of the discriminator gradients (w.r.t the inputs) be 1. The objective function of the WGAN with this updated soft constraint (termed a gradient penalty) is shown in Eq. 2.

$$L^{gp} = L^w + \lambda \mathbb{E}_{\tilde{x} \sim P_f} (\|\nabla D_{\Omega}(\tilde{x})\|_2 - 1)^2 \quad (2)$$

Each sample  $\tilde{x} \sim P_f$  is generated as a convex combination of points from  $P_r$ ,  $P_f$  (i.e., sampled from the line connecting points from  $P_r$ ,  $P_f$ ).  $\lambda$  enforces the strictness of the gradient penalty.

#### B. Contrastive Learning (CL)

The paradigm of contrastive learning (CL) has recently demonstrated highly effective results across a diverse set of disciplines and tasks, especially in computer vision [4], [6], [24]. The goal of CL is to impose structure on latent representations learned by a model (M). This is often achieved using soft penalties (e.g., additional loss terms) that influence

representations generated by M to be structured so representations of *related* instances are closer together relative to instances that are known to be *unrelated*. Most CL losses are set in a *self-supervised* context where *relatedness* is generated via augmentations of an instance and two distinct instances are considered to be unrelated.

Recently, [7] proposed *supervised contrastive learning* (SupCon), which is an extension of the CL paradigm to supervised (classification) settings. A model trained with SupCon on a labeled dataset learns latent representations grouped by *class labels* while also forcing separation in representations between instances belonging to different classes (i.e., low intra-class separation and high inter-class separation of latent representations).

Consider a dataset of instances  $\mathcal{D} = \{(x_1, y_1), \dots, (x_m, y_m)\}$  such that  $x_i \in \mathbb{R}^{b \times l}$  and  $y_i \in \mathcal{C}$  is the label of  $x_i$  and  $\mathcal{C}$  is the set of class labels. Then, the supervised contrastive loss is defined by Eq. 3.

$$L^{sup} = \sum_{x_i \in \mathcal{D}} \frac{-1}{|Pos(i)|} \sum_{x_k \in Pos(i)} \log \frac{\exp(z_i \cdot z_k / \tau)}{\sum_{j \in Q(i)} \exp(z_i \cdot z_j / \tau)} \quad (3)$$

Here,  $z_i \in \mathbb{R}^{h \times 1}$  is the latent representation of  $x_i$  generated by model M.  $Pos(i) = \{x_k \in \mathcal{D} | y_k == y_i \wedge k \neq i\}$  is the set of instances that form the ‘positive set’ for  $x_i$ .  $Q(i) = \{\mathcal{D} \setminus x_i\}$ .  $\tau \in \mathbb{R}^+$  is a hyperparameter. We employ Eq. 3 for CL but with labels generated in a self-supervised manner.

#### C. Uncertainty Quantification (UQ)

Quantifying decision uncertainty is critical to the success of real-world machine learning (ML) frameworks. It is of special relevance in the current setting of anomaly detection wherein the confidence of a model in its decision additionally indicates the urgency of a potential alert issued by the model. While traditional ML models yield point predictions, Bayesian ML provides a framework for capturing model uncertainty. One such UQ approach [25], can be considered to approximate Gaussian Processes with neural network models. This approach termed Monte-Carlo Dropout entails running a monte-carlo sampling (during inference) of a trained model by randomly masking a set of learned weights of the model each time (i.e., *dropout* [26]). This is akin to sampling from the *approximate posterior* which leads to uncovering the model’s predictive distribution. Inferring the predictive distribution is one of the methods to quantify model uncertainty with Bayesian neural networks.

### IV. PROBLEM FORMULATION

We shall now describe the various facets of our novel human-in-the-loop anomaly detection framework CAAD-EF. Fig. 2 details the overall architecture of CAAD-EF.

#### A. Self Supervised Anomaly Detection with Negative Transformations

The core of the proposed framework is the Contrastive Adversarial Anomaly Detection (CAAD) model. The structure of the CAAD model resembles a WGAN with gradient

<sup>2</sup>words ‘critic’, ‘discriminator’ are used interchangeably in the paper.

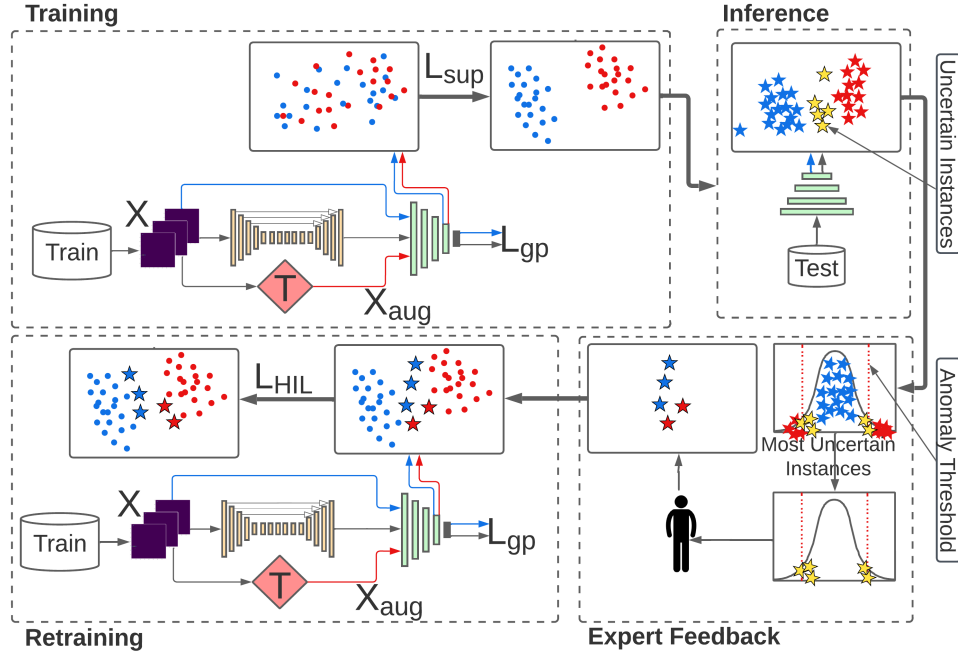


Fig. 2. The full architecture of the human-in-the-loop CAAD-EF anomaly detection framework. (Training): The framework consists of a WGAN-GP with an uncertainty-aware discriminator trained with supervised contrastive learning (SupCon) to impose structure in the latent space. Labeled data required for SupCon is obtained by applying ‘negative transformations’ on a benign set of instances to generate corresponding anomalous instances. (Inference): During inference, the model yields a prediction (*anomaly*:red star or *benign*:blue star) for every instance, accompanied by the prediction uncertainty. (Expert Feedback): Uncertain instances (yellow stars) are isolated and passed to an *expert* to uncover their true labels. (Re-Training): The pre-trained WGAN-GP model is then fine-tuned with this additional expert feedback to further improve its representations learned thereby leading to improved anomaly detection performance and decreased prediction uncertainty.

penalty (WGAN-GP) as described in section III comprising a generator  $G_\theta$  and a discriminator  $D_\Omega$ . In addition to GAN-based training, we also train CAAD discriminator with CL to impose explicit structure on the learned latent representations and improve representation learning. The CL technique employed is similar to supervised contrastive learning (SupCon) detailed in section III. However, SupCon requires a labeled dataset. To generate a labeled dataset  $\mathcal{D}$ , we assume the existence of a training set without any anomalies. Let this set be denoted  $\mathcal{D}_b = \{(x_1, y_1), \dots, (x_m, y_m)\}$ , such that  $y_i = 0, \forall (x_i, y_i) \in \mathcal{D}_b$ . We apply a negative transformation  $T(\cdot)$  to violate the normalcy of every instance  $x_i \in \mathcal{D}_b$  to obtain a corresponding set of anomalous instances  $\mathcal{D}_a = \{(x_1, y_1), \dots, (x_m, y_m)\}$  such that  $y_i = 1, \forall (x_i, y_i) \in \mathcal{D}_a$ . Now let us consider  $\mathcal{D} = \{\mathcal{D}_a, \mathcal{D}_b\} = \{(x_1^a, y_1^a), \dots, (x_m^a, y_m^a), (x_1^b, y_1^b), \dots, (x_m^b, y_m^b) | y_i^a = 1 \wedge y_i^b = 0 \forall i\}$ . Then we can leverage Eq. 3 to directly train the CAAD discriminator with CL (specifically SupCon).

$$L^{CAAD} = L^{gp} + \alpha L^{sup} \quad (4)$$

Eq. 4 represents the objective employed to train the CAAD model to learn effective representations of benign and negatively transformed ‘anomalous’ instances via CL. Here,  $\alpha$  governs the effect of the supervised contrastive loss on the discriminator representations.

### B. Inferring Decision Uncertainty with CAAD-UQ

In order to maximize the effect of expert feedback on model performance, we are required to isolate an *effective* set of instances for which to solicit feedback. To this end, we define this *effective* set of instances as those for which the model is the most uncertain in its prediction. Hence CAAD, trained to learn effective representations as defined in section IV-A, is augmented to quantify its prediction uncertainty using the popular Monte-Carlo dropout technique (see section III-C). This variant of CAAD augmented with uncertainty quantification capability is termed CAAD-UQ. Concretely, the model structure of CAAD discriminator is augmented by including *dropout* in each layer of the model to yield CAAD-UQ. Let  $D_{\Omega^*}^L$  represent the first  $L$  layers of the discriminator of a trained CAAD-UQ model where training happens according to Eq. 4. Further, let  $d_i = D_{\Omega^*}^L(x_i)$ , then,  $\{d_i^j\}_{j=1 \dots k}$  represents the set of ‘k’ monte-carlo sampled embeddings obtained from  $D_{\Omega^*}^L(x_i)$ . CAAD-UQ employs the mean of the Monte-Carlo embeddings, denoted  $\bar{d}_i$  as the representation inferred for an instance  $x_i \in \mathcal{D}$ .

Every Monte-Carlo embedding  $d_i^j$  generated by  $D_{\Omega^*}^L(x_i)$  is subjected to a *scoring mechanism* (section IV-D) whereby a prediction  $\hat{y}_i^j \in \{0, 1\}$  is obtained. Here  $\hat{y}_i^j = 0$  indicates a benign classification and  $\hat{y}_i^j = 1$  indicates an anomalous classification of  $x_i$  at MC sample  $j$ . Prediction uncertainty as quantified by CAAD-UQ for  $\bar{d}_i$  is outlined in Eq. 6

$$u_{i,c} = |\{\hat{y}_i^j | j \in \{1, 2, \dots, k\} \wedge \hat{y}_i^j = c\}| \text{ where } c \in \{0, 1\} \quad (5)$$

$$\mu_i = 1 - \frac{\max(u_{i,0}, u_{i,1})}{k} \quad (6)$$

### C. Leveraging Expert Feedback

Now, we have formulated a method to calculate an uncertainty measure  $\mu_i$  for any instance  $x_i$ . For  $\{x_i\} \in \mathcal{D}$  for which we want to make predictions, if  $\mu_i \approx 1 \forall x_i$ , then we can be sure that the model predictions are reliable. However, if this is not true, we further retrain CAAD-UQ for a small number of epochs using a set of *effective* instances determined using  $\mu_i$  and their corresponding feedback from an expert on these instances, along with the original training set. We call this model CAAD-EF since this is a contrastive adversarial anomaly detection model trained from expert feedback.

For a particular class  $c$ , we define the supervised contrastive loss in Eq. 7.

$$L^{\text{supclass}}(\mathcal{D}, c) = L^{\text{sup}}(\mathcal{D}) \quad \forall x_i : y_i = c \quad (7)$$

$L^{\text{supclass}}$  is used to only bring instances of one class  $c$  together and away from all other classes, in contrast with  $L^{\text{sup}}$  which brings each instance close to each other instance of the same class and away from instances of all other classes.

Let  $X$  denote a set of benign instances. From the set of inferences yielded by CAAD-UQ, we select the top ‘h’% most uncertain instances  $X^{\text{HIL}}$ , based on  $\mu_i$  (Eq. 6) as the *effective* set of instances and showcase them to an expert to receive feedback. This feedback gives us  $\{X_{\text{anom}}^{\text{HIL}}, X_{\text{ben}}^{\text{HIL}}\}$  where  $X_{\text{anom}}^{\text{HIL}}$  and  $X_{\text{ben}}^{\text{HIL}}$  are the set of instances labeled by an expert as anomalous and benign respectively. We then incorporate an additional loss term in the loss function of CAAD-UQ and retrain the model for a small number of epochs. Let  $X_{\text{aug}} = T(X)$  where  $T$  is a class of transformations,  $\mathcal{D}_1 = \{X_{\text{anom}}^{\text{HIL}}, X\}$ ,  $\mathcal{D}_2 = \{X_{\text{ben}}^{\text{HIL}}, X_{\text{aug}}\}$ ,  $\mathcal{D}_3 = \{X_{\text{ben}}^{\text{HIL}}, X_{\text{anom}}^{\text{HIL}}\}$ . We define the HIL loss  $L^{\text{HIL}}$  in Eq 8.

$$L^{\text{HIL}} = \alpha_1 L^{\text{supclass}}(\mathcal{D}_1, c = 1) + \alpha_2 L^{\text{supclass}}(\mathcal{D}_2, c = 0) + \alpha_3 L^{\text{supclass}}(\mathcal{D}_3, c = 0) \quad (8)$$

where the first term in  $L^{\text{HIL}}$  helps bring  $X_{\text{anom}}^{\text{HIL}}$  together while also pushing it far away from  $X$ , the second term helps bring  $X_{\text{ben}}^{\text{HIL}}$  together while pushing it far away from  $X_{\text{aug}}$  and the third term helps bring  $X_{\text{ben}}^{\text{HIL}}$  together and pushes it away from  $X_{\text{anom}}^{\text{HIL}}$ . Hence the overall loss term for the retraining model CAAD-EF is given below.

$$L_D = L^{\text{CAAD}} + L^{\text{HIL}} \quad (9)$$

### D. Anomaly Detection

Training our model gives us meaningful embeddings. Here we define how we use these embeddings for identifying anomalies.

**Scoring function:** We define a scoring function that can be used to determine if an instance is an anomaly or not. We

adopt the scoring mechanism used in [13]. Consider a set of instances used during training. We cluster them into  $m$  different clusters and obtain their cluster centroids as  $\{x_m\}$ . For every test instance  $x_i$ , the score is calculated as below.

$$s_{x_i} = \max(\cosine(D_{\Omega^*}^L(x_i), D_{\Omega^*}^L(x_m))) \quad \forall x_m \quad (10)$$

**Anomaly threshold:** Consider a validation set  $x_v$  and a distribution  $P$  of anomaly scores  $s_{x_v}$ .

$$\theta = \arg_{\theta} \{P(s_{x_v} < \theta) = \phi\} \quad (11)$$

where  $\phi$  is the strictness parameter which can be tuned to control the rate of false positives and false negatives. When  $s_{x_i}$  exceeds  $\theta$ , then we call  $x_i$  an anomaly.

## V. EXPERIMENTAL SETUP

We consider several wireless emission activity datasets as well as the well-known MNIST computer vision dataset for evaluation. The wireless emission activity datasets consist of metadata describing detected radio emissions observed over the air in a known radio frequency (RF) environment. Metadata describes a range of aspects including detection time, frequency, bandwidth, signal type, and signal power, and is streamed from an edge sensor into an Elasticsearch database for archival. Anomalies consist primarily of new emitters coming online or exhibiting new behavior (e.g. hopping) in a band with otherwise orderly patterned behavior, or the disappearance (e.g. failure) of emitters that are otherwise regularly present.

### A. Dataset Description

**LTW1:** Long-term wireless emission metadata in the 800-900MHz band collected for a span of 2 months from a first geographical location with a frequency scanning receiver. We consider a 2D 80x80 bin density feature formed from quantized bandwidth and frequency features from these emissions over 3-minute intervals. This forms 11670, 5002, 7146 time intervals in a sequential manner for training, validation, and test sets respectively. We denoise training and validation set densities by setting values of bins with a probability of occurrence less than 0.0005 to zero. The test set contains 3894 benign and 3738 anomalies which also includes hopping anomalies.

**LTW2:** Long-term wireless emission metadata (similar to LTW1) collected from a second geographical location. Input is preprocessed similar to 80x80 bin density features of LTW1. Data spans a time interval of 10 days and forms 1645, 706, 1310 sequential time intervals for training, validation, and test sets respectively. The test set contains 786 benign and 724 anomalies.

**STW1:** Short-term wireless emission metadata collected from a third geographical location comprising short-time high-rate observations of 900MHz cellular and ISM bands. Input similar to 80x80 bin density features of LTW1 but with a 1-second interval. One 4G LTE signal (i.e. cellular base station) goes offline (signal drop) at around 198 seconds into the dataset. 154, 39, 198 are the number of training, validation, and

testing instances respectively. The test set contains 94 benign and 104 anomalies.

We note that the datasets LTW1, LTW2, STW1 are collected using on-the-ground sensors and depict real-world benign and anomalous behavior of communication network traffic.

**MNIST:** This is a standard image dataset [27] for machine learning research comprising images of hand-written digits. The training and validation set consists of 4089 and 1753 images of the number ‘4’ (benign class) respectively. During testing, all other classes of digits are considered anomalies. The test set contains 982 benign and 9018 anomalous images leading to an imbalanced evaluation setup.

### B. Baselines

We evaluated several baselines that are either state-of-the-art or closely related to CAAD. All of them are explained in this section.

**Isolation Forest** [28]: A popular benchmark ensemble method for anomaly detection wherein partitions are created in data such that each data point is isolated. During such partitioning, an anomalous data instance isolates itself much easier compared to a benign instance. We employed 100 base estimators.

**One Class SVM (OC-SVM)** [29]: OC-SVMs learn a hypersphere that encompasses points from a single class and any point that falls outside of this hypersphere is considered an outlier. The kernel that was used in the algorithms is a radial basis function kernel.

**UNetGAN** [30]: GAN model with UNet as a generator, and convolutional network used for the discriminator. The GAN model is trained using Wasserstein loss and gradient penalty.

**fAnoGAN** [11]: A state-of-the-art anomaly detection model based on Wasserstein GAN-GP. It comprises a two-stage AD framework wherein the first stage involves WGAN-GP being trained to translate samples from a noise distribution to outputs of the process of interest. The second stage employs the pre-trained WGAN-GP to train an encoder network to learn an ‘inverse mapping’ of the WGAN-GP generator. The anomaly score is calculated as a function of error between intermediate representations of input data and generator output.

**Contrasting Shifted Instances (CSI)** [13]: A state-of-the-art anomaly detection deep neural network model which employs traditional self-supervised contrastive learning with a novel contrastive task comparing an instance to *distributionally shifted* versions of itself. Anomaly detection occurs through a novel anomaly scoring mechanism.

After finding the anomaly score, all the baselines and CAAD follow the same procedure as mentioned in IV-D to detect anomalies.

### C. Evaluation Metrics

We employ multiple evaluation metrics to provide a holistic quantitative evaluation of model performance on the task of anomaly detection. Specifically, we separately report the *F1 scores* for correctly detecting benign and anomaly instances as well as a *weighted average* of the two F1 scores. Further,

we also report the Area Under the Receiver Operating Characteristic (AUROC) metric which is explicitly dependent on the false positive rates (FPR) of the models. We explicitly report AUROC to investigate whether models have low FPRs (thereby high AUROC) values which are imperative for an effective anomaly detection model. Finally, as we also deal with imbalanced datasets (see section V-A), we also monitor the Area Under the Precision-Recall Curve (AUPRC) metric which is known to complement AUROC well by alleviating biases due to data imbalance.

### D. Model & Training Details

**Model details:** The backbone of CAAD-EF is a WGAN with gradient penalty (WGAN-GP). The generator of this WGAN-GP is a UNet autoencoder comprising 5 down convolutional layers (each with kernel size 4, batch normalization, and leaky-ReLU), 5 same convolutional layers (each with kernel size 3, maxpooling, batch normalization, and leaky-ReLU) and 5 up-convolutional layers (each with kernel size 4 batch normalization and ReLU). Discriminator has five convolutional layers, each followed by instance normalization, leaky-ReLU (negative slope of 0.2), and a dropout layer with a dropout probability of 0.5.

**Training details:** Our models are trained for 100 epochs with a batch size of 32, Adam optimizer ( $\beta_1 = 0, \beta_2 = 0.9$ ), and learning rate of  $1e^{-4}$  for both the generator and the discriminator. For the gradient penalty, we use a  $\lambda$  value of 10. The weighting coefficients  $\alpha, \alpha_1, \alpha_2$  and  $\alpha_3$  are set to 1 during training. The negative transformation we have employed is *salt noise* for the network datasets (LTW1, LTW2, STW1) and  $90^\circ$  rotations for MNIST. Strictness parameter  $\phi = 0.99$  and number of training clusters  $m = 1$  are used during validation. During retraining, we train the model only for 7 epochs. Considering that feedback from experts is not easy to obtain and is expensive, we use a  $h$  value of 5 (corresponding to 5% of the most uncertain instances) during retraining. Although we only explore single-round expert feedback in our experiments, if more feedback can be afforded, our framework can also be used to support multi-round expert feedback for active learning.

## VI. RESULTS AND DISCUSSION

We now investigate the performance of our novel CAAD-EF anomaly detection framework. Our detailed analysis entails a rigorous quantitative and qualitative performance evaluation. The specific research questions we ask are as follows:

- How does our CAAD model perform relative to the existing state-of-the-art (SOTA) for anomaly detection?
- Can we augment CAAD to successfully incorporate expert feedback (CAAD-EF) to improve the quality of learned representations?
- How does each facet of our novel CAAD-EF framework contribute towards the overall performance?

TABLE I  
SUMMARY OF RESULTS.

| Data  | Model            | Benign F1   | Anomaly F1  | AUROC       | AUPRC       | Avg.Wt. F1  |
|-------|------------------|-------------|-------------|-------------|-------------|-------------|
| LTW1  | Isolation Forest | 0.75        | 0.47        | 0.88        | 0.83        | 0.61        |
|       | OC-SVM           | 0.41        | 0.7         | 0.86        | 0.81        | 0.55        |
|       | CSI              | 0.75        | 0.2         | 0.61        | 0.53        | 0.48        |
|       | fAnoGAN          | 0.69        | 0.18        | 0.8         | 0.8         | 0.44        |
|       | fAnoGAN**        | 0.68        | 0.04        | 0.85        | 0.84        | 0.37        |
|       | UnetGAN          | 0.74        | 0.41        | 0.86        | 0.89        | 0.58        |
|       | CAAD             | <b>0.93</b> | <b>0.9</b>  | <b>0.97</b> | <b>0.97</b> | <b>0.92</b> |
| STW1  | Isolation Forest | 0.64        | 0           | 0.49        | 0.57        | 0.3         |
|       | OC-SVM           | 0.59        | 0.79        | 0.97        | 0.98        | 0.7         |
|       | CSI              | 0.03        | 0.81        | 0.37        | 0.58        | 0.44        |
|       | fAnoGAN          | 0.85        | 0.72        | 0.95        | 0.93        | 0.78        |
|       | fAnoGAN**        | 0.83        | 0.79        | 0.96        | 0.63        | 0.81        |
|       | UnetGAN          | 0.85        | 0.9         | <b>1.0</b>  | <b>1.0</b>  | 0.88        |
|       | CAAD             | <b>0.92</b> | <b>0.94</b> | <b>1.0</b>  | <b>1.0</b>  | <b>0.93</b> |
| LTW2  | Isolation Forest | 0.75        | 0.02        | 0.63        | 0.71        | 0.46        |
|       | OC-SVM           | 0.34        | 0.59        | 0.74        | 0.78        | 0.44        |
|       | CSI              | <b>0.84</b> | 0.27        | 0.63        | 0.3         | 0.61        |
|       | fAnoGAN          | 0.75        | 0.14        | 0.7         | 0.58        | 0.51        |
|       | fAnoGAN**        | 0.76        | 0.6         | 0.73        | 0.63        | 0.7         |
|       | UnetGAN          | 0.73        | 0.36        | 0.64        | 0.5         | 0.58        |
|       | CAAD             | 0.77        | <b>0.73</b> | <b>0.86</b> | <b>0.83</b> | <b>0.75</b> |
| MNIST | Isolation Forest | 0.28        | 0.63        | 0.88        | 0.59        | 0.6         |
|       | OC-SVM           | 0.56        | 0.96        | 0.91        | 0.62        | 0.92        |
|       | CSI              | 0.55        | 0.9         | 0.9         | 0.81        | 0.87        |
|       | fAnoGAN          | 0.51        | 0.88        | <b>0.98</b> | <b>1.0</b>  | 0.84        |
|       | fAnoGAN**        | 0.31        | 0.65        | 0.95        | 0.99        | 0.62        |
|       | UnetGAN          | 0.5         | 0.89        | 0.93        | 0.99        | 0.85        |
|       | CAAD             | <b>0.76</b> | <b>0.97</b> | 0.93        | <b>1.0</b>  | <b>0.95</b> |

#### A. CAAD Anomaly Detection Performance

At the outset, we shall investigate the anomaly detection capability of the CAAD model which forms the backbone of our proposed, novel CAAD-EF framework. Specifically, we evaluate the anomaly detection performance of CAAD across four datasets comprising diverse characteristics and anomalies (see section V-A).

Table I details the anomaly detection performance comparison of CAAD with several well-accepted state-of-the-art (SOTA) anomaly detection models. Across all the datasets and types of anomalies, CAAD achieves a mean performance improvement of **92.84%** as evidenced by the anomaly *F1 score* metric. CAAD also achieves an overall mean performance improvement of **59.39%** across three of the four datasets where CAAD is the best performing model (i.e., combined performance on benign and anomaly detection) as demonstrated by the weighted average F1 score metric.

**False Positives:** An important facet of a robust and practically useful anomaly detection framework is its ability to minimize ‘false alarms’. To investigate this behavior, we report AUROC (see V-C) which explicitly is a function of the false positive rate (FPR).

CAAD yields consistently high AUROC values (indicative of its low FPR i.e., it produces very few false alarms). CAAD yields the highest AUROC values in three out

of the four datasets. We must note that in the case of the MNIST dataset, the AUROC of CAAD (i.e., **0.93**) is competitive and amenable for use in real-world AD applications.

Due to the variegated nature of data imbalance in our experiments (see section V-A for data support statistics) we also evaluate the AUPRC metric (as a complement to AUROC under data imbalance). We notice that CAAD is the best performing<sup>3</sup> across all datasets (including MNIST) as per the AUPRC metric.

**Network Anomaly Detection:** CAAD is able to detect extremely ‘weak’ anomalous signatures associated with activity in irregular parts of the spectrum being monitored. This is specifically evidenced by the superior performance of CAAD on datasets LTW1 and

LTW2, both of which contain attack signatures generated by devices that inappropriately access unused regions of the band being monitored. The superior performance of CAAD in anomaly detection on the STW1 dataset which consists of the ‘signal drop’ anomaly (described in section V-A), also demonstrates the versatility of the CAAD model to detect different types of irregularities in different bands across the communication spectrum. We notice that the CSI model has a higher benign F1 score but lower overall wt.Avg. F1 score (as

<sup>3</sup>accompanied by fAnoGAN on MNIST, UNetGAN on STW1

it underperforms on the corresponding anomaly detection task) for the LTW2 dataset. CAAD in contrast yields more stable results for detecting both benign and anomalous instances across all datasets.

**MNIST Anomaly Detection:** We once again notice that CAAD is able to outperform all other SOTA models for anomaly detection on the MNIST dataset. This result is significant, as it is indicative of the generic nature and flexibility of the proposed solution in addressing variegated anomaly detection tasks. We once again notice that CAAD yields the best anomaly detection F1 score (**1.04%** improvement over next best model OC-SVM) and the best weighted average F1 score (**3.26%** improvement over next best model OC-SVM). CAAD is also the best performing for the benign instance recognition (indicated by benign F1 score). The inconsistency in model performance across the benign and AD tasks is once again evident in the context of skewed results in the OC-SVM (fails to detect benign instances accurately). Hence, we once again note (as evidenced by the Wt. Avg. F1 score, Benign F1 score, and Anomaly F1 score) that CAAD yields the best performance on the MNIST AD task.

**SOTA Models:** Standard AD models like Isolation Forest and OC-SVM perform poorly, especially for the challenging *network AD* task. They are unable to identify the subtle anomalous patterns of interest. The fAnoGAN variants showcase unstable performance across the two tasks of benign and AD as evidenced by the large differences in the F1 scores for each dataset thereby rendering them practically ineffective for use as real-world AD frameworks. CSI which is a recent SOTA AD model that also employs contrastive learning significantly underperforms relative to CAAD (avg. performance improvement by Wt. Avg. F1 score **58.78%**) across all the datasets.

Overall, experiments in Table I indicate the superior representation learning and AD capability of CAAD on small and large, balanced and imbalanced datasets comprising multiple different types of anomalies.

### B. Anomaly Detection with Expert Feedback

Real-world systems can often benefit from incorporating valuable expert knowledge to influence their representation learning capabilities. To this end, in an effort to further improve the performance of CAAD, we augment it with the capacity to incorporate expert feedback received in the form of instance labels for a limited set of instances. The resulting framework CAAD-EF comprises an augmentation to the discriminator of the CAAD model enabling it to characterize its prediction uncertainties (see section IV). This uncertainty-aware model (CAAD-UQ) is trained in a similar fashion to CAAD. Once trained, CAAD-UQ yields inferences on unseen instances accompanied by its prediction uncertainty. We select ‘h%’ of the most uncertain instances as inferred by CAAD-UQ to be labeled by an expert. This labeled set of instances is leveraged in a feedback loop to fine-tune the

representations learned by CAAD-UQ, thus yielding a holistic human-in-the-loop anomaly detection CAAD-EF framework.

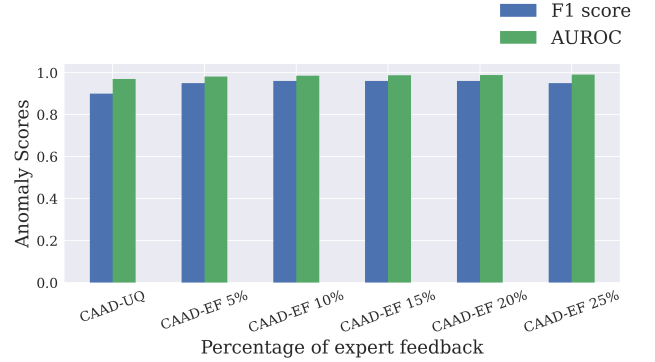


Fig. 3. Improvement in Anomaly F1 scores and AUROC values are observed as we increase the percentage of expert feedback 0% (CAAD-UQ) to 25% feedback. We notice that the model is able to show noticeable improvement in the F1 score even with 5% expert feedback.

**Effect of Expert Feedback (Quantitative Evaluation):** To investigate the effectiveness of expert feedback in the context of large and small datasets, we select LTW1 and STW1 datasets to inspect CAAD-EF performance. Table II showcases the experimental results. In this table, CAAD-EF 95% is the CAAD-EF evaluated only on a test set with expert feedback instances removed. We see that incorporating expert feedback (i.e., CAAD-EF) yields a significant performance improvement in the case of large (LTW1) and small (STW1) training datasets. Specifically, we notice that incorporating expert feedback on a small subset of uncertain instances (we select instances corresponding to 5% of the most uncertain test predictions as candidates for expert feedback) yields an average performance improvement of **4.17%** over the next best model on the AD task (i.e., improvement in Anomaly F1 score) across both datasets. This indicates that the CAAD-EF benefits significantly from expert feedback in the context of different anomalies and data sizes. Additionally, CAAD-EF also showcases a **3.79%** performance improvement over CAAD (i.e., the variant without explicit feedback) in recognizing benign instances (i.e., improvement in Benign F1 score) across both the datasets showcasing a holistic performance improvement. These results are indicative of a highly effective, holistic and generic AD solution. For completeness, we further characterized the effect of model performance of CAAD-EF with the increase in expert feedback (Fig. 3). Figure 4 shows the values of uncertainty for the 5% most uncertain instances before retraining (from CAAD-UQ) and after retraining (from CAAD-EF). We can clearly notice the improvement in uncertainty scores after retraining. This result further clarifies the improved performance in CAAD-EF.

**Effect of Expert Feedback (Qualitative Evaluation):** To further corroborate our claim of improved representation learning of CAAD-EF due to expert feedback, we also analyze the evolution of the discriminator embeddings of CAAD-EF before and after fine-tuning with expert feedback. Fig 5

TABLE II  
IMPACT OF FINE TUNING WITH EXPERT FEEDBACK.

| Data | Model       | Benign F1 | Anomaly F1 | AUROC | AUPRC | Avg.Wt. F1 |
|------|-------------|-----------|------------|-------|-------|------------|
| LTW1 | CAAD        | 0.93      | 0.9        | 0.97  | 0.97  | 0.92       |
|      | CAAD-UQ     | 0.92      | 0.9        | 0.97  | 0.98  | 0.91       |
|      | CAAD-EF     | 0.94      | 0.94       | 0.98  | 0.98  | 0.94       |
|      | CAAD-EF 95% | 0.95      | 0.94       | 0.98  | 0.98  | 0.95       |
| STW1 | CAAD        | 0.92      | 0.94       | 1     | 1     | 0.93       |
|      | CAAD-UQ     | 0.93      | 0.94       | 1     | 1     | 0.94       |
|      | CAAD-EF     | 0.98      | 0.98       | 1     | 1     | 0.98       |
|      | CAAD-EF 95% | 0.98      | 0.99       | 1     | 1     | 0.99       |

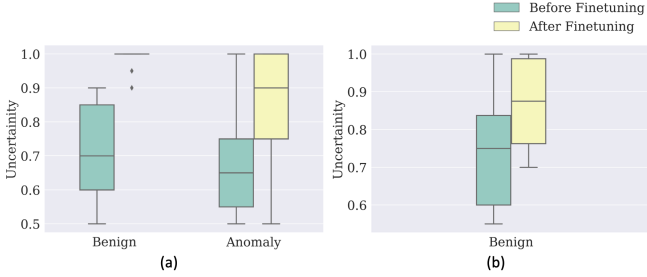


Fig. 4. These figures display box plots of uncertainty values of human-in-the-loop (HIL) instances before and after retraining. Figure (a) shows results from the LTW1 dataset and figure (b) shows results from the STW1 dataset. Figure (b) does not contain values for HIL anomalies as there were no HIL anomalies. Here, an uncertainty value of 1 indicates high certainty of prediction and an uncertainty value of 0 indicates low certainty of prediction.

showcases t-SNE plots of embeddings inferred by the CAAD-EF discriminator. Fig. 5a shows the representations inferred by CAAD-UQ before expert feedback; color indicates ground truth labels (red: anomalies, blue: benign). We notice clearly the effect of the contrastive learning employed to train the discriminator, leading to a clear separation of anomalous and benign regions in the plot. In Fig. 5b we notice CAAD-UQ is uncertain about a significant number of points in the inference set. This region of uncertainty (ROU - indicated by the dotted black circle in Fig. 5b) is identified and 5% of most uncertain instances (as indicated by CAAD-UQ) are supplied to the expert for feedback. These expert-labeled instances are highlighted as red (expert label: anomaly) or blue (expert label: benign) points in Fig 5c. The model is fine-tuned with the full training set and the updated sets of points to produce new uncertainty estimates (Fig. 5e) wherein we see that the model is significantly less uncertain in the ROU (which has shrunk significantly). Finally, we notice that the instances that were supplied by the expert as feedback have achieved significant separation and gravitated towards their respective cluster centroids (Fig. 5f) thereby leading to improved model performance in the CAAD-EF framework.

### C. Q3. Ablation Study CAAD-EF

We have thus far verified through rigorous qualitative and quantitative experiments, the effectiveness of our proposed CAAD-EF framework for AD. CAAD-EF consists of

multiple facets and it is important to characterize the effect of each. Hence, we conduct a detailed ablation study of the proposed CAAD-EF framework. Table III details the results. We notice from the table that the CAAD-EF model is dependent on each facet of its pipeline for effective representation learning with the most significant drop in performance occurring due to the removal of the contrastive learning based model training. We notice that the performance of our proposed CAAD framework is a function of the effect of contrastive learning and adversarial training. The performance is further improved with the inclusion of expert feedback (CAAD-EF). Removal of the UNet blocks from the generator also lead to deterioration in performance, primarily due to decrease in the generator learning capability. Finally, we once again notice the significant drop in performance (0.94 to 0.91 Wt. Avg. F1) when expert feedback is ignored. The results in Table III further reinforce the effectiveness of CAAD-EF framework for the task of AD.

## VII. CONCLUSION

In this paper we have introduced CAAD, a novel AD framework employing contrastive learning in an adversarial setup. We have demonstrated through rigorous experiments that our proposed method outperforms SOTA AD baselines and achieves a **92.84%** improvement for AD in wireless communication networks as well as in more generic AD contexts. We further propose CAAD-EF which is a variant of CAAD capable of incorporating expert feedback and evaluated its effectiveness through several qualitative and quantitative experiments. Incorporating expert feedback gives a performance boost of 4.19% over CAAD. Finally, we also highlight the importance of each facet of our proposed CAAD-EF framework through a detailed ablation study. Moving forward we shall augment CAAD-EF with more sophisticated uncertainty quantification techniques and leverage the power of our model for real-time human-in-the-loop AD applications, especially those plagued by covariate shift. The proposed models can be evaluated on more datasets to establish generalizability. We shall evaluate our methods on more sophisticated anomalies and also venture into adopting our models to detect sequential anomalies.

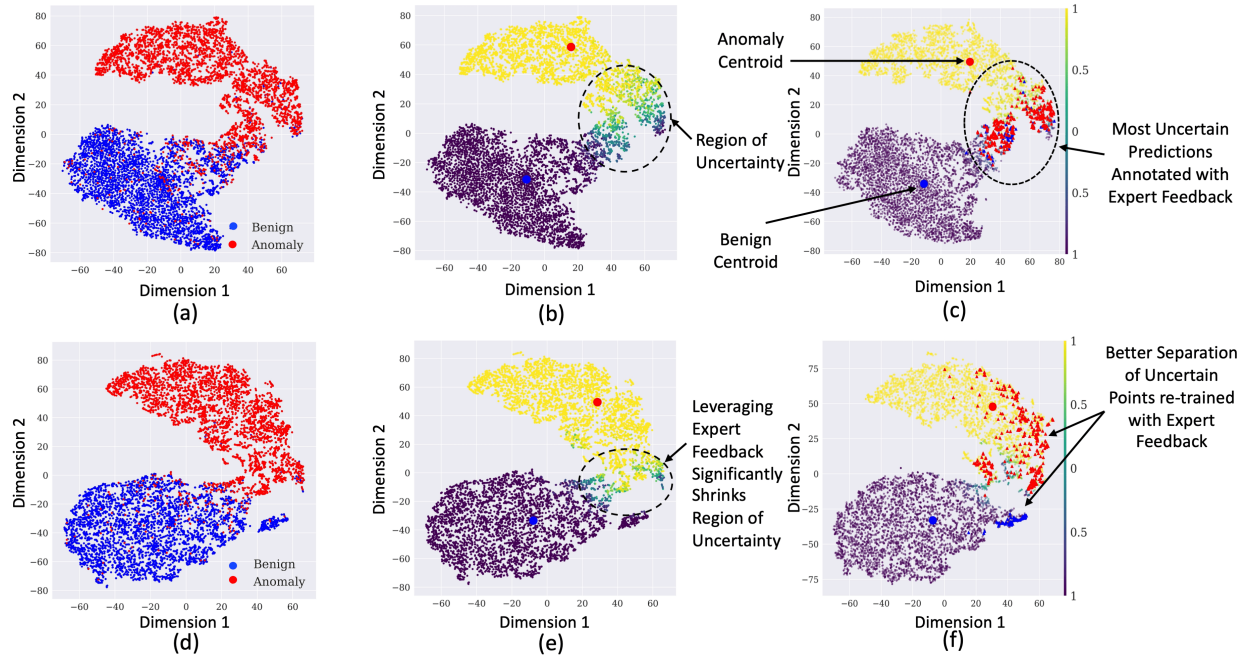


Fig. 5. Figures (a) - (f) qualitatively represent the effect of incorporating human feedback in our proposed CAAD-EF framework. (a) Depicts t-SNE embeddings of our CAAD-UQ model discriminator, colored by the ground truth labels with anomalies colored red and benign points colored blue. (b) Showcases the same t-SNE embeddings as Fig. 5a but colored by the uncertainties obtained from the CAAD-UQ model (yellow: anomaly with low prediction uncertainty, purple: benign with low prediction uncertainty, green regions indicate uncertain instances;). We notice a highly focused but sizeable ‘Region of Uncertainty’ (ROU) indicated by the dotted black circle. (c) Ground truth labels of points in the ROU as specified by the expert (red: anomalous points, blue: benign points). (d) Depicts (similar to Fig. 5a) updated t-SNE embeddings yielded by the CAAD-UQ discriminator after fine-tuning with expert feedback for 5% of most uncertain instances. (e) Updated uncertainty estimates of CAAD-UQ post fine-tuning, we see a significant reduction in ROU (indicated by a dotted black circle) compared to Fig. 5b (f) CAAD-UQ model fine-tuned with expert feedback results in greater separation between benign (blue) and anomalous instances (red) in ROU. This consequently also leads to the overall decrease in decision uncertainty as observed in Fig. 5e.

TABLE III  
INCREMENTAL ABLATION OF CAAD-EF  
EF: RETRAINING AFTER EXPERT FEEDBACK, UQ: UNCERTAINTY QUANTIFICATION AND CL: CONTRASTIVE LEARNING.

| Model                           | Benign F1   | Anomaly F1  | AUROC       | AUPRC       | Avg.Wt. F1  |
|---------------------------------|-------------|-------------|-------------|-------------|-------------|
| CAAD-EF                         | <b>0.94</b> | <b>0.94</b> | <b>0.98</b> | <b>0.98</b> | <b>0.94</b> |
| CAAD-EF w/o EF                  | 0.92        | 0.9         | 0.97        | 0.98        | 0.91        |
| CAAD-EF w/o EF, UQ              | 0.93        | 0.9         | 0.97        | 0.97        | 0.92        |
| CAAD-EF w/o EF, UQ, CL          | 0.74        | 0.41        | 0.86        | 0.89        | 0.58        |
| CAAD-EF w/o EF, UQ, CL, UNet    | 0.72        | 0.28        | 0.84        | 0.83        | 0.5         |
| CAAD-EF w/o EF, UQ, CL, WGAN-GP | 0.73        | 0.32        | 0.83        | 0.8         | 0.53        |

## REFERENCES

- [1] “Wi-fi and non wi-fi interference — metageek,” <https://www.metageek.com/training/resources/wifi-and-non-wifi-interference/>, (Accessed on 10/15/2022).
- [2] I. Goodfellow, J. Pouget-Abadie, M. Mirza, B. Xu, D. Warde-Farley, S. Ozair, A. Courville, and Y. Bengio, “Generative adversarial networks,” *Communications of the ACM*, vol. 63, no. 11, pp. 139–144, 2020.
- [3] L. Jing and Y. Tian, “Self-supervised visual feature learning with deep neural networks: A survey,” *IEEE transactions on pattern analysis and machine intelligence*, vol. 43, no. 11, pp. 4037–4058, 2020.
- [4] S. Chopra, R. Hadsell, and Y. LeCun, “Learning a similarity metric discriminatively, with application to face verification,” in *CVPR’05*, vol. 1. IEEE, 2005, pp. 539–546.
- [5] J. Jeong and J. Shin, “Training gans with stronger augmentations via contrastive discriminator,” *arXiv preprint arXiv:2103.09742*, 2021.
- [6] T. Chen *et al.*, “A simple framework for contrastive learning of visual representations,” in *ICML*. PMLR, 2020, pp. 1597–1607.
- [7] P. Khosla, P. Teterwak, C. Wang, A. Sarna, Y. Tian, P. Isola, A. Maschinot, C. Liu, and D. Krishnan, “Supervised contrastive learning,” *Advances in Neural Information Processing Systems*, vol. 33, pp. 18 661–18 673, 2020.
- [8] M. Arjovsky, S. Chintala, and L. Bottou, “Wasserstein generative adversarial networks,” in *International conference on machine learning*. PMLR, 2017, pp. 214–223.
- [9] C. Zhou and R. C. Paffenroth, “Anomaly detection with robust deep autoencoders,” in *Proceedings of the 23rd ACM SIGKDD international conference on knowledge discovery and data mining*, 2017, pp. 665–674.
- [10] T. Schlegl *et al.*, “Unsupervised anomaly detection with generative adversarial networks to guide marker discovery,” in *International conference on information processing in medical imaging*. Springer, 2017, pp. 146–157.
- [11] T. Schlegl, P. Seeböck, S. M. Waldstein, G. Langs, and U. Schmidt-Erfurth, “f-anogan: Fast unsupervised anomaly detection with generative adversarial networks,” *Medical image analysis*, vol. 54, pp. 30–44, 2019.
- [12] H. Cho, J. Seol, and S.-g. Lee, “Masked contrastive learning for anomaly detection,” *arXiv preprint arXiv:2105.08793*, 2021.

- [13] J. Tack, S. Mo, J. Jeong, and J. Shin, "Csi: Novelty detection via contrastive learning on distributionally shifted instances," *Advances in neural information processing systems*, vol. 33, pp. 11 839–11 852, 2020.
- [14] T. Reiss and Y. Hoshen, "Mean-shifted contrastive loss for anomaly detection," *arXiv preprint arXiv:2106.03844*, 2021.
- [15] S. Das, W.-K. Wong, T. Dietterich, A. Fern, and A. Emmott, "Incorporating expert feedback into active anomaly discovery," in *2016 IEEE 16th International Conference on Data Mining (ICDM)*. IEEE, 2016, pp. 853–858.
- [16] N. Görmitz, M. Kloft, K. Rieck, and U. Brefeld, "Toward supervised anomaly detection," *Journal of Artificial Intelligence Research*, vol. 46, pp. 235–262, 2013.
- [17] G. Pang, L. Cao, L. Chen, and H. Liu, "Learning representations of ultrahigh-dimensional data for random distance-based outlier detection," in *Proceedings of the 24th ACM SIGKDD international conference on knowledge discovery & data mining*, 2018, pp. 2041–2050.
- [18] G. Pang, C. Shen, and A. van den Hengel, "Deep anomaly detection with deviation networks," in *Proceedings of the 25th ACM SIGKDD international conference on knowledge discovery & data mining*, 2019, pp. 353–362.
- [19] G. Pang, A. van den Hengel, C. Shen, and L. Cao, "Toward deep supervised anomaly detection: Reinforcement learning from partially labeled anomaly data," in *Proceedings of the 27th ACM SIGKDD Conference on Knowledge Discovery & Data Mining*, 2021, pp. 1298–1308.
- [20] X. Han, X. Chen, and L.-P. Liu, "Gan ensemble for anomaly detection," *arXiv preprint arXiv:2012.07988*, vol. 7, no. 8, 2020.
- [21] Y. Choi, H. Lim, H. Choi, and I.-J. Kim, "Gan-based anomaly detection and localization of multivariate time series data for power plant," in *2020 IEEE international conference on big data and smart computing (BigComp)*. IEEE, 2020, pp. 71–74.
- [22] H. Cheng, H. Liu, F. Gao, and Z. Chen, "Adgan: A scalable gan-based architecture for image anomaly detection," in *2020 IEEE 4th Information Technology, Networking, Electronic and Automation Control Conference (ITNEC)*, vol. 1. IEEE, 2020, pp. 987–993.
- [23] I. Gulrajani *et al.*, "Improved training of wasserstein gans," *NeurIPS*, vol. 30, 2017.
- [24] J. Zbontar *et al.*, "Barlow twins: Self-supervised learning via redundancy reduction," in *ICML*. PMLR, 2021, pp. 12 310–12 320.
- [25] Y. Gal and Z. Ghahramani, "Dropout as a bayesian approximation: Representing model uncertainty in deep learning," in *international conference on machine learning*. PMLR, 2016, pp. 1050–1059.
- [26] N. Srivastava *et al.*, "Dropout: a simple way to prevent neural networks from overfitting," *JMLR*, vol. 15, no. 1, pp. 1929–1958, 2014.
- [27] L. Deng, "The mnist database of handwritten digit images for machine learning research," *IEEE Signal Processing Magazine*, vol. 29, no. 6, pp. 141–142, 2012.
- [28] F. T. Liu, K. M. Ting, and Z.-H. Zhou, "Isolation forest," in *2008 ICDM*. IEEE, 2008, pp. 413–422.
- [29] Y. Wang, J. Wong, and A. Miner, "Anomaly intrusion detection using one class svm," in *Proceedings from the Fifth Annual IEEE SMC Information Assurance Workshop, 2004*. IEEE, 2004, pp. 358–364.
- [30] O. Ronneberger, P. Fischer, and T. Brox, "U-net: Convolutional networks for biomedical image segmentation," in *International Conference on Medical image computing and computer-assisted intervention*. Springer, 2015, pp. 234–241.

## APPENDIX

### A. Wireless Dataset Description

Using Software Defined Radio (SDR), we gather metadata about wireless signals, particularly FM signals. This metadata is in the form of JSON with each instance containing information about packets of signals and a timestamp. Two features we have used from this metadata are center frequency and bandwidth. We create 80x80 bins with bandwidth on the x-axis and frequency on the y-axis and populate the count of packets falling into each bin for a period of 3 minutes. This gives us a time series of 80x80 images. For context, the maximum count of packets per pixel in the LTW1 dataset

is 98 and the maximum count of packets per pixel in the LTW2 dataset is 201. Also, the mean of maximum count of packets per pixel per image is 20.5 for LTW1 and 107.1 for LTW2. This indicates that LTW2 is dense compared to LTW1. Min-max normalization based on the global min and max of the count of packets per pixel of the training set is performed. Once such normalized images are gathered, we denoise the training set by masking out pixels that have a probability of having a non-zero value of  $< 0.0005$ .

### B. Types of Wireless Anomalies

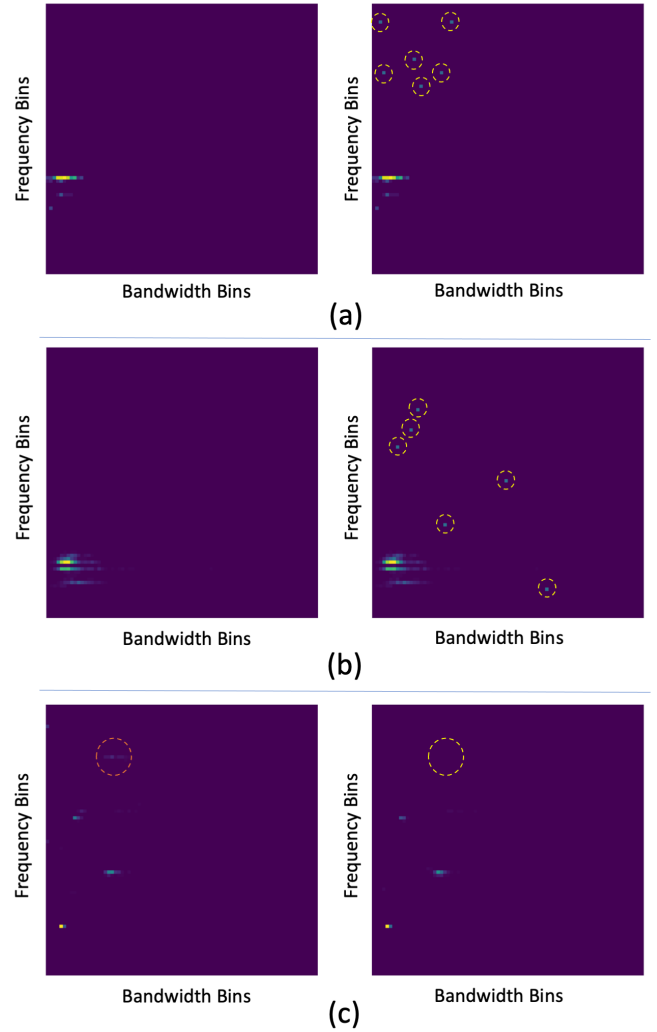


Fig. 6. These are examples of preprocessed wireless emission activity data that we input into our models. The left figures indicate benign instances and the right figures indicate corresponding anomalous instances. Anomalies are annotated with dashed yellow circles. Figure (a) is a sample from the LTW1 dataset. Anomalies in the right figure of (a) are 7x amplified in order to improve visibility. Figure (b) is a sample from the LTW2 dataset. Anomalies in the right figure of (b) are 30x amplified in order to improve visibility. Figure (c) is a sample from the STW1 dataset. In the left figure in (c), the orange circle points to the signal that goes missing in the right figure (Drop anomaly).

- 1) **Hopper Anomalies:** In this type of anomaly, frequency hopper signals are transmitted. This creates activity in different regions of the 80x80 image. Examples of such hopper anomalies are shown in Figures 6a and 6b.
- 2) **Drop Anomalies:** In this type of anomaly, an LTE signal in the cellular band goes offline at around 198 seconds into the dataset. We use until 170 seconds of data from training and the rest, with anomalies for testing. This removes a region of activity from the 80x80 image. Examples of a drop anomaly is shown in Figure 6c.
- 3) **Naturally occurring anomalies:** In the training set, as mentioned in Section A, we mask out pixels that have a probability of having a non-zero value of  $< 0.0001$ . However, we do not do this in the testing set and we instead label such images as anomalies.

### C. Anomaly Injection

- 1) **Injection of hopper anomalies:** The available number of real-world hopper anomalies was 60 packets with different bandwidths and frequencies for each packet. These 60 packets were then grouped into numbers of 6 which effectively produced 10 different anomaly signatures. Now, every anomaly signature contains 6 anomalies with each having a count (density) of 1. We use these anomaly signatures as template anomalies and inject (add) them in test instances without anomalies while also keeping a copy of the original test instance without anomalies. Before anomaly injection, the template is min-max normalized using the global min and max of the count of packets per pixel of the entire training set. As LTW2 has max of the count of packets per pixel of the entire training set value as 201 and since our anomalies have a density of 1, during min-max normalization, the injected anomalies become very subtle. This is one explanation for the relatively low anomaly F1 scores in LTW2 compared to other datasets. Figure 6b shows anomalies amplified by 30x in order to be visible to the naked eye.
- 2) **Injection of Drop Anomalies:** To inject drop anomalies, the LTE signal is manually turned off.